JOURNAL OF GEOPHYSICAL RESEARCH, VOL. 115, B04313, doi:10.1029/2009JB006716, 2010

On the robustness of global radially anisotropic surface wave tomography

A. M. G. Ferreira,[1,2] J. H. Woodhouse,[3] K. Visser,[4] and J. Trampert[5]

Received 23 June 2009; revised 27 October 2009; accepted 18 November 2009; published 23 April 2010.

[1] A number of recent global tomographic studies have modeled three dimensional variations in the parameters of radial anisotropy. As yet there is limited agreement among such studies, suggesting significant uncertainties in the models, which could lead to divergent geodynamical interpretations. In this study we assess the robustness of lateral variations in radial anisotropy globally in the upper mantle and in the transition zone to determine the extent to which anisotropic parameters are constrained by a data set of over 10,000,000 fundamental and higher mode surface wave dispersion measurements. We carry out inversions for isotropic and radially anisotropic shear wave velocity, systematically changing regularization and using three different crustal models to remove the effects of the crust on the data. Using crustal corrections from different crustal models has an impact on the data fit comparable or larger than that obtained by including lateral variations of radial anisotropy in the modeling. Moreover, the use of crustal corrections from different *a priori* crustal models may lead to different images of radial anisotropy suggesting divergent geodynamical interpretations. This work suggests that the three-dimensional determination of global radial anisotropy in the Earth's mantle using surface wave dispersion data is still an ongoing experiment.

Citation: Ferreira, A. M. G., J. H. Woodhouse, K. Visser, and J. Trampert (2010), On the robustness of global radially anisotropic surface wave tomography, *J. Geophys. Res.*, *115*, B04313, doi:10.1029/2009JB006716.

1. Introduction

[2] When detected, seismic anisotropy can potentially be an indicator of mantle flow and thus can help us discriminating different geodynamical processes and competitive thermo-chemical convective models of the Earth's interior. Deformation processes in the mantle can lead to detectable seismic anisotropy, which could result for example from lattice-preferred orientation (LPO) of minerals [*McNamara et al.*, 2002] or from the alignment of structural elements, including layers of melt [*Williams and Garnero*, 1996]. While observations of anisotropy at shallow depths may indicate "frozen" anisotropy over geological timescales [*Silver*, 1996], anisotropy at greater depths could reflect the current mantle strain rate field [e.g., *Vinnik et al.*, 1992].

[3] Numerous studies have confirmed the presence of anisotropy in the Earth's uppermost mantle. Early evidence for radial anisotropy in the upper mantle came from the observed discrepancy between Rayleigh and Love waves [*Anderson*, 1961; *Aki and Kaminuma*, 1963; *McEvilly*, 1964]. These observations led to the incorporation of radial anisotropy from the Mohorovicic discontinuity down to 220 km depth in the global one-dimensional (1-D) reference Earth model PREM [*Dziewonski and Anderson*, 1981]. With the increasing availability of high-quality digital seismograms recorded by global seismic networks and with the growth of computing power, various approaches have been devised to map the three-dimensional radially anisotropic structure globally.

[4] Seismic surface waves are particularly well suited to investigate radial anisotropy in the upper mantle and in the transition zone globally because their sensitivity to earth structure is approximately constant along the raypath, which, combined with good raypath coverage, provides a better sampling of these regions than body waves. While fundamental mode surface wave data provide the best constraints on seismic structure in the uppermost mantle, using higher mode data greatly improves the depth resolution of Earth models [e.g., *Ritsema et al.*, 1999].

[5] Several studies have mapped lateral variations of radial anisotropy in the upper mantle globally by the simultaneous inversion of fundamental Rayleigh and Love data [*Nataf et al.*, 1984, 1986; *Ekström and Dziewonski*, 1998; *Montagner and Tanimoto*, 1991; *Shapiro and Ritzwoller*, 2002]. Recently, higher-mode surface wave data have been added to global three-dimensional tomographic inversions for radial anisotropy [e.g., *Gung et al.*, 2003; *Panning and Romanowicz*, 2004; *Marone et al.*, 2007].

[1] School of Environmental Sciences, University of East Anglia, Norwich, UK.
[2] ICIST, Instituto Superior Técnico, Technical University of Lisbon, Lisbon, Portugal.
[3] Department of Earth Sciences, University of Oxford, Oxford, UK.
[4] Built Environment and Geosciences, TNO, Utrecht, Netherlands.
[5] Department of Earth Sciences, Utrecht University, Utrecht, Netherlands.

0148-0227/10/2009JB006716

Table 1. Phase Velocity Measurements Used in This Study

Branch	Rayleigh Waves		Love Waves	
	Period Range (s)	Number of Measurements	Period Range (s)	Number of Measurements
Fundamental	374 – 35	3,988,786	375 – 35	1,141,006
First overtone	274 – 35	1,088,232	177 – 35	622,605
Second overtone	110 – 35	980,774	115 – 35	432,831
Third overtone	99 – 35	706,291	79 – 35	250,458
Fourth overtone	69 – 35	454,353	63 – 35	120,520
Fifth overtone	56 – 35	289,743	56 – 35	59,598
Sixth overtone	51 – 35	129,792	–	0

[6] Progress in anisotropic tomography has been slower than elastic tomography due to the difficulties of extracting the anisotropic signal from seismic waves in the presence of significant elastic effects due to wave propagation in a heterogeneous Earth. Radially anisotropic global velocity models tend to agree at long wavelengths only [e.g., *Kustowski et al.*, 2008], suggesting large uncertainties in these models. Discrepancies between radially anisotropic models may result from data uncertainties, insufficient data coverage, or from the use of varying modeling techniques. One of the difficulties in estimating radial anisotropy in the mantle is linked to the crust. In addition to the mantle, surface waves are strongly sensitive to crustal structure, so the effects of the crust must be taken into account when modeling radial anisotropy either by including crustal parameters in the inversions or by carrying out crustal corrections based on an *a priori* crustal model. The latter is the approach often followed in global surface wave tomographic studies and it has been shown that inaccurate crustal corrections may lead to large errors in the models [e.g., *Marone and Romanowicz*, 2007]. Since Love waves are most affected by the crust, radially anisotropic models are particularly susceptible to incorrect crustal corrections [*Bozdag and Trampert*, 2007]. Previous global studies often rely on choosing a particular *a priori* crustal model and on applying (linear or nonlinear) crustal corrections based on that model. Some recent regional and upper mantle studies explicitly attempt to quantify the trade-off between unknown crustal structure and inferred radial anisotropy. For example, *Shapiro and Ritzwoller* [2002] and *Shapiro et al.* [2004] carry out Monte Carlo inversions that yield uncertainty estimates on seismic velocities in the crust and upper mantle, which depend on assessing the uncertainties in the imposed constraints on the crust. Moreover, detailed regional models of the crust and upper mantle can be built using short-period surface waves, including group velocity measurements [e.g., *Pasyanos and Walter*, 2002] and, with recent developments in ambient noise tomography, short-period (T = 8–20s) Rayleigh and Love fundamental dispersion measurements [e.g., *Yang et al.*, 2008].

[7] In this study we use a very large set of fundamental mode and overtone surface wave dispersion measurements to investigate the global isotropic and radially anisotropic shear wave velocity structure of the upper mantle and of the transition zone. We carry out inversion experiments and a detailed analysis of data misfit in order to identify quantitatively to what extent our data set requires deviations of radial anisotropy from PREM. Rather than using one single crustal model to calculate crustal corrections, we use three independent crustal models to assess the effect of using different crustal corrections in the modeling. Furthermore, we assess the impact on the data fit of allowing lateral variations in P wave velocity in the inverse modeling.

2. Data

[8] In this study we use surface wave phase velocity anomalies with respect to PREM of fundamental and higher-mode Love and Rayleigh waves up to the fifth and sixth overtone, respectively. We merge the measurements of *Visser et al.* [2007a] with those of *van Heijst and Woodhouse* [1999] and of *Ekström et al.* [1997] into a data set with a total of over 10,000,000 minor-arc phase-velocity measurements, for multimode Rayleigh and Love waves with wave periods between T = 35s and T = 375s, with good global coverage (Table 1).

[9] Over half of the measurements are for overtones. This provides us with a dispersion data set significantly larger than those used in global studies of radial anisotropy to date. *Visser et al.* [2007a] showed that their measurements agree well with the measurements made by *van Heijst and Woodhouse* [1999]. We have carried out additional comparisons of the various data sets and checked that they are consistent with each other before combining all the measurements into an expanded data set. It is expected that using such a large, consistent data set will reduce the null-space and the impact of regularization in the inversions.

3. Methodology

3.1. Theory

[10] A transversely isotropic medium with a vertical axis of symmetry can be described by the density ρ and by the parameters $A = \rho V_{PH}^2$, $C = \rho V_{PV}^2$, $L = \rho V_{SV}^2$, $N = \rho V_{SH}^2$ and $F = \eta\rho\,(V_{PH}^2 - 2V_{SV}^2)$ [*Love*, 1927; *Takeuchi and Saito*, 1972]. In this study we parameterize our model in terms of the isotropic S velocity structure, $v_S^2 = \frac{1}{2}(V_{SV}^2 + V_{SH}^2)$, and the anisotropic parameter $\zeta_s = \frac{v_{SH}^2 - v_{SV}^2}{2v_S^2}$. We express the perturbations in density and in P velocity using the scaling relations $\frac{\delta\rho}{\rho} = 0.4\frac{\delta V_S}{V_S}$ [*Anderson et al.*, 1968] and $\frac{\delta V_P}{V_P} = 0.5\frac{\delta V_S}{V_S}$ [e.g., *Robertson and Woodhouse*, 1995], respectively. We neglect sensitivity to variations in the intermediate parameter η and we do not consider perturbations to the depth of seismic discontinuities in the reference model. Moreover, we also neglect azimuthal anisotropy, as its modeling introduces a large number of model parameters to the modeling. The effect of potential azimuthal anisotropy is reduced by the excellent azimuthal coverage, so that in principle azimuthal variations will be

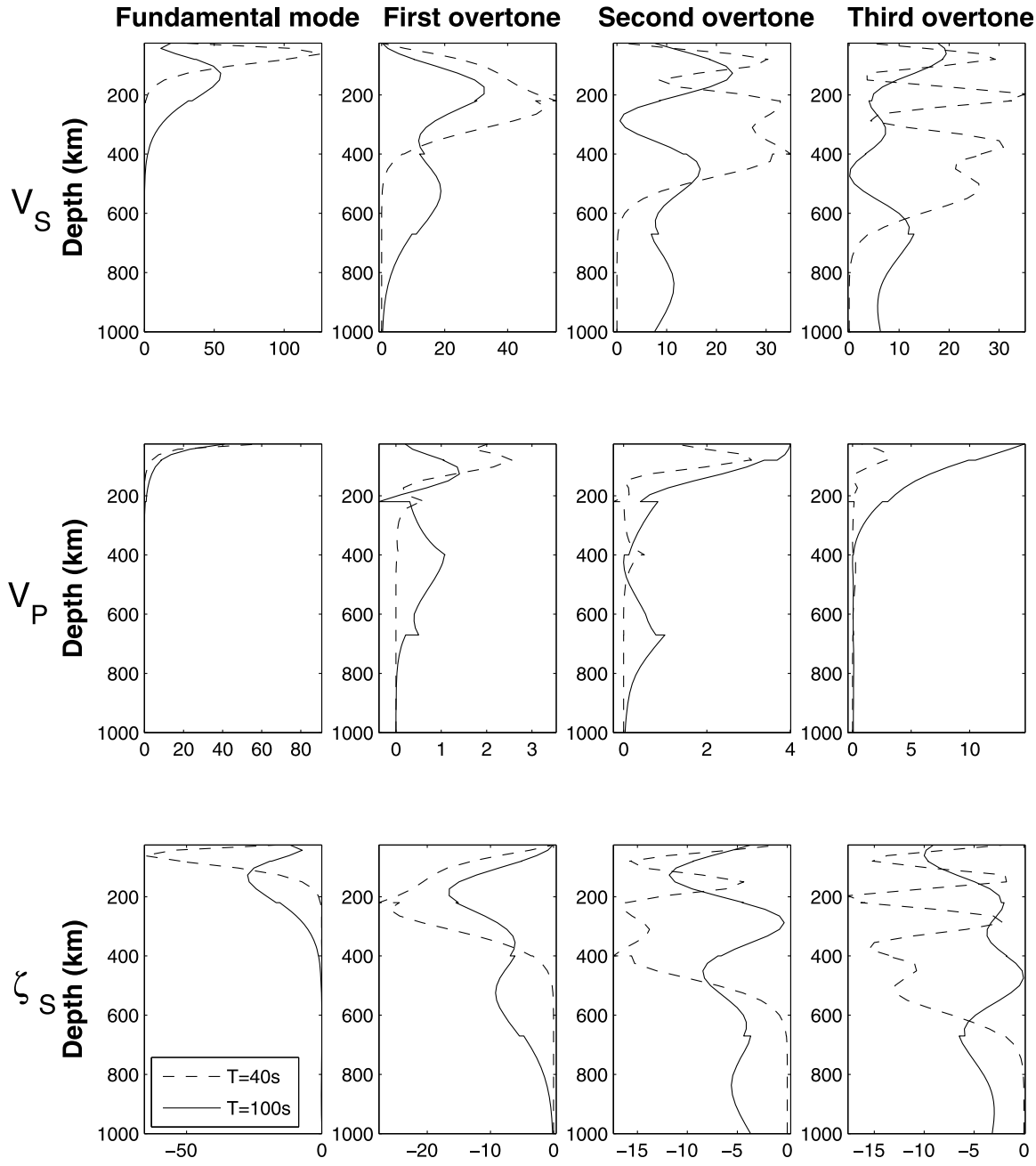

Figure 1. Depth sensitivity kernels that relate phase velocities of the fundamental and the first, second and third overtone Rayleigh waves (top) to isotropic S velocity structure, (middle) to P velocity structure and (bottom) to radial anisotropy for the PREM model. Solid lines are for wave periods with T = 100s and dashed lines are for T = 40s.

averaged out at each point of the model. Nevertheless, recent work by *Visser et al.* [2007b] suggests that at least for phase velocity maps, the trade-off between azimuthal anisotropic and isotropic terms is small, so that future 3-D imaging of azimuthal anisotropy based on the data set used in this study should be possible.

[11] We use the great circle approximation to calculate sensitivity kernels that linearly relate surface wave phase anomalies and Earth's structure [e.g., *Woodhouse and Dziewonski*, 1984]. Figures 1 and 2 show sensitivity kernels of fundamental and higher mode Rayleigh and Love waves calculated using PREM. The sensitivities shown are the derivatives of the eigenfrequency with respect to $\frac{\delta V_S}{V_S}$, $\frac{\delta V_P}{V_P}$ and $\frac{\delta \zeta_s}{\zeta_s}$ for a given mode. As expected, for shorter periods the phase velocities of the same mode branch are sensitive to shallower structure and the kernels become more complex with increasing overtone number. The sensitivity to changes in P velocity is generally smaller than to changes in S velocity. Nevertheless, for the third higher mode with T = 100s, P velocity anomalies contribute significantly to the phase velocity perturbations.

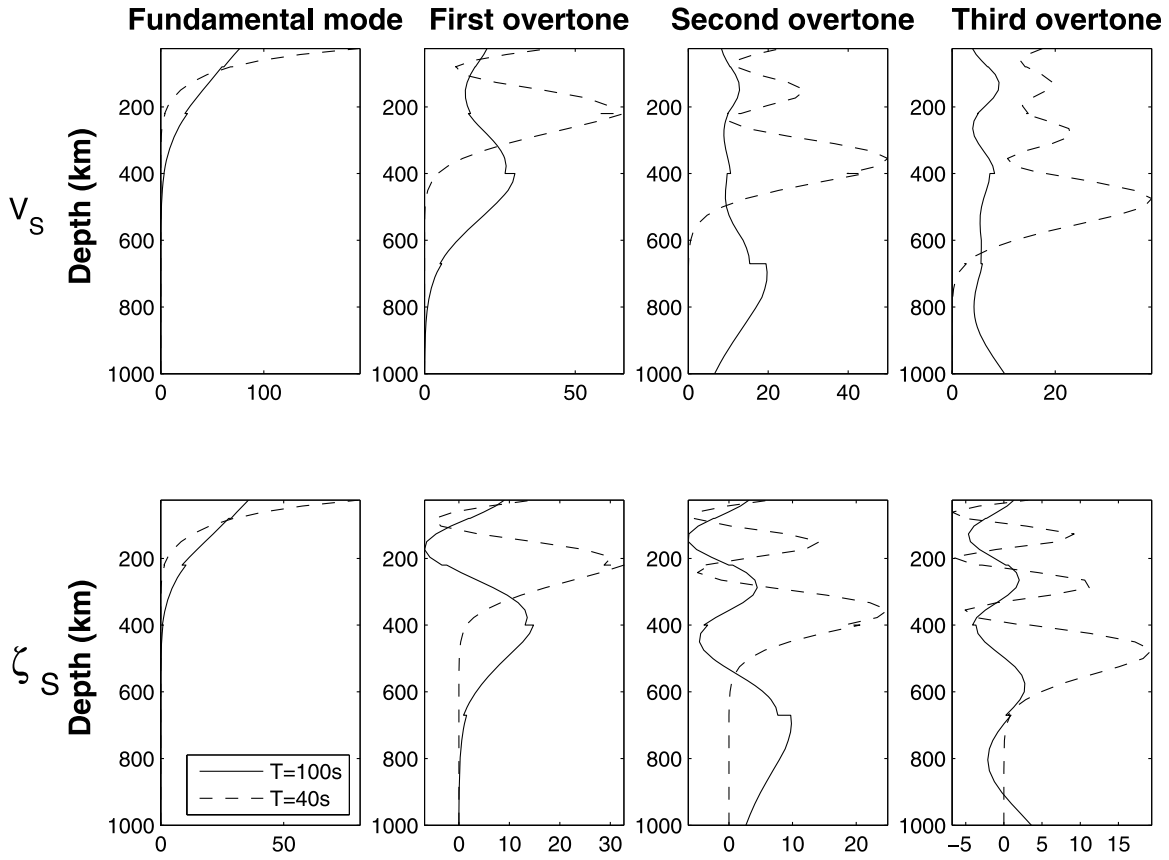

Figure 2. Same as Figure 1, but for Love waves.

3.2. Model Parameterization

[12] We parameterize the variations of isotropic shear wave velocity and of radial anisotropy horizontally in terms of spherical harmonic basis functions up to degree 20 (corresponding to a lateral resolution at the surface of about 2,000 km). The variations in the radial direction are parameterized using 15 spline functions from the crust down to 2000 km (Figure 3). The spacing of the splines is smallest in the uppermost mantle to allow for the highest vertical resolution at shallow depths, where the resolving power of the data is highest (the vertical resolution is of ≈60 km at the surface and of ≈300 km at the greatest depths).

3.3. Inversion

[13] The model coefficients are determined by formulating an inverse problem, which minimizes the least squares misfit between the predictions and the data. The data are inverted simultaneously for isotropic and radially anisotropic perturbations from the 1-D reference Earth model PREM. We apply regularization through horizontal gradient damping; no explicit radial damping is imposed in the inversions. We construct the inner product matrix of the data derivatives A^TA by projecting the sensitivity kernels into the horizontal and radial basis functions and we use eigenvalue decomposition to invert it to obtain damped least squares model solutions. We carry out inversions for a total of 13,230 parameters (half of them for isotropic structure and the other half for radially anisotropic structure).

[14] As explained in section 3.1, we model the data using the great circle approximation, which is computationally efficient and thus convenient to analyze our large data set and to carry out many inversion experiments involving the determination of a large number of model parameters. Although more sophisticated theories have been developed that should allow us to obtain more accurate results in the future [e.g., *Sieminski et al.*, 2007], these remain computationally expensive, especially for global-scale inversions involving millions of measurements as in this study.

3.4. Crustal Corrections

[15] Surface waves are sensitive to crustal structure, so accurate crustal corrections are essential to prevent mapping crustal features into mantle tomographic images [e.g., *Bozdag and Trampert*, 2007; *Marone and Romanowicz*, 2007]. We remove the effects of the crust by using *a priori* global models of the crust. To determine the crustal correction for the phase velocity measurements, we superimpose the *a priori* crustal model on PREM and calculate local eigenfrequencies for the modes used in the modeling in each block of a grid sampling the surface of the Earth. Whenever the *a priori* crust is thinner than PREM's crust, we extrapolate PREM's uppermost mantle structure up to the bottom of the new crust. We expand the gridded local eigenfrequency perturbations with respect to PREM in spherical harmonics and subtract the contribution of the crust from each individual measurement. We correct for the *a priori* crustal structure using spherical harmonics only up to the maximum angular order used in the tomographic

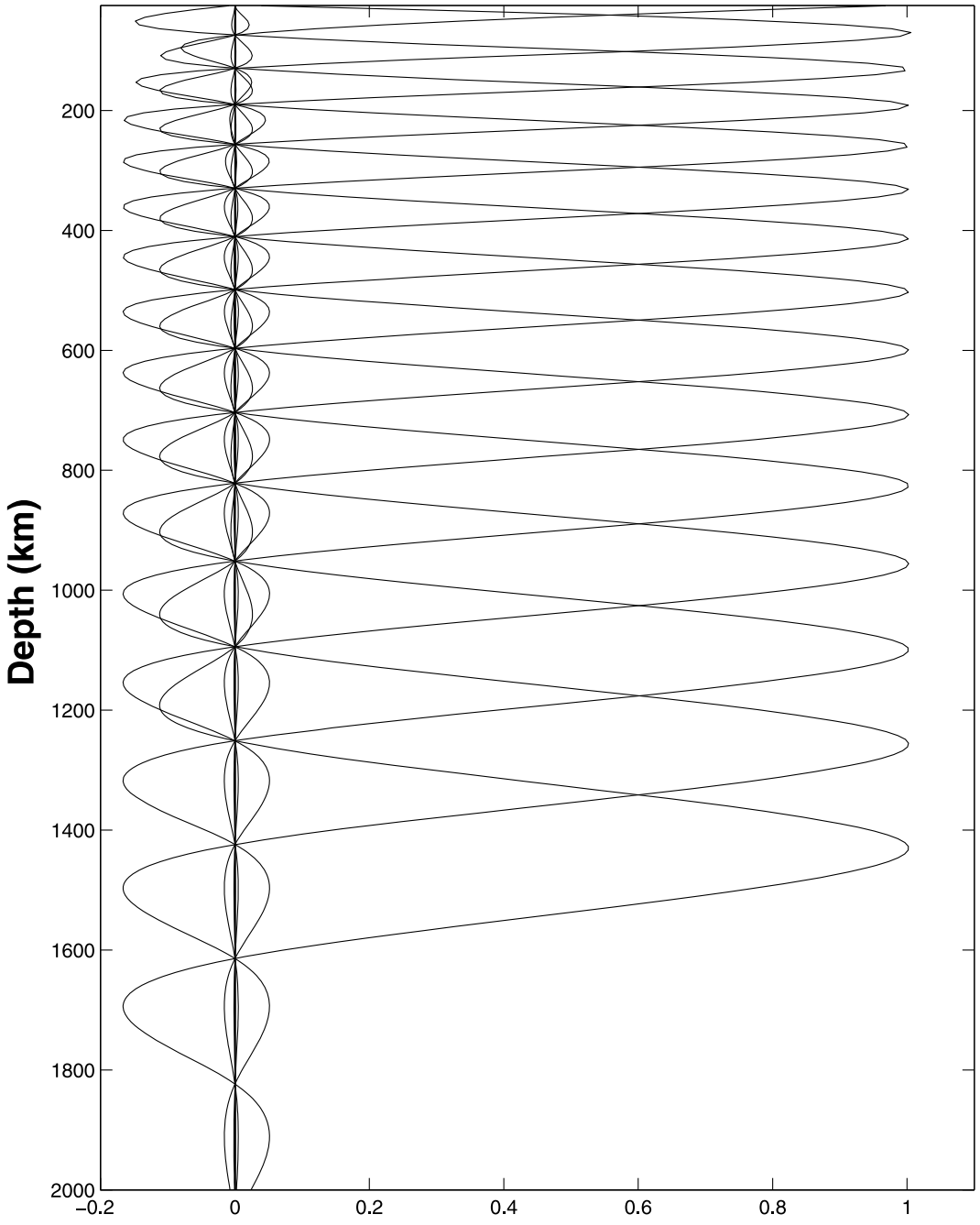

Figure 3. Fifteen spline functions used to parameterize the depth dependence of perturbations in S velocity, in P velocity and in radial anisotropy.

modeling even if the crustal model is defined for shorter lateral wavelengths. In this study we use three different crustal models to calculate crustal corrections: the crustal model CRUST2.0 [*Bassin et al.*, 2000], the crustal part of the model 3SMAC [*Nataf and Ricard*, 1996] and the crustal model by *Meier et al.* [2007], which we shall refer to as CRUST07. These three crustal models are constrained using different approaches and thus are useful to test the effect of using different crustal corrections when modeling radial anisotropy. CRUST2.0 is based on a large compilation of seismic refraction data and of ice and sediment thickness. 3SMAC is an *a priori* model based on tectonics, heat flow, and geophysical knowledge. CRUST07 consists of an average shear wave velocity for the crust and a Moho depth obtained by inverting fundamental mode phase and group velocities using a neural network approach. Figures 4 and 5 show Rayleigh and Love phase velocity distributions associated with these three crustal models for waves with different periods. As expected, Love waves are more sensitive to the crust (e.g., see Figures 1 and 2). The strongest signal in the phase velocity distributions is related to the difference between oceans and continents. In general, continental regions are slow and oceanic regions are fast. Fundamental modes are strongly affected by the crustal structure, but the sensitivity of

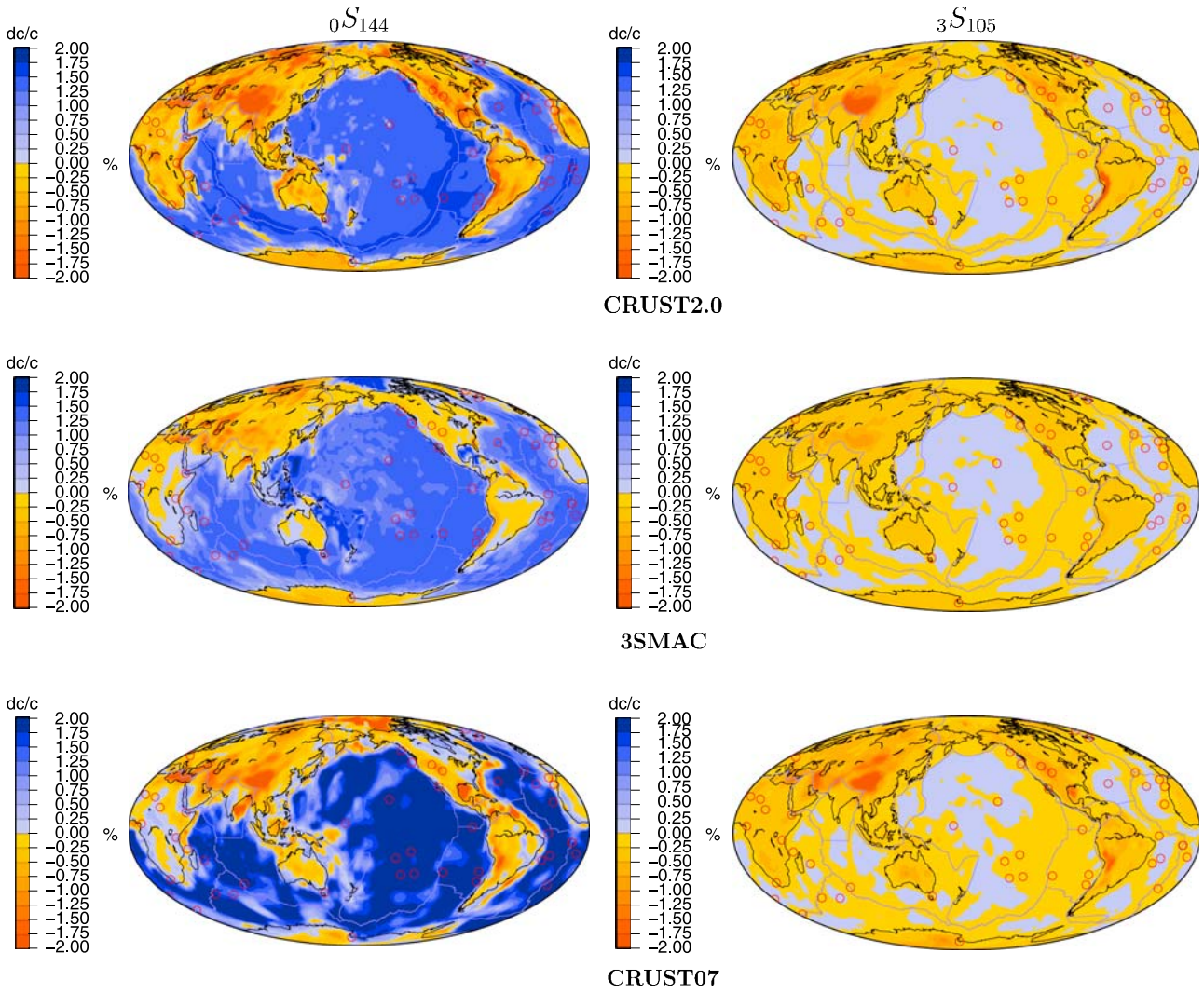

Figure 4. Rayleigh wave phase velocity distributions associated with the crustal model (top) CRUST2.0, (middle) 3SMAC and (bottom) CRUST07 (left) for the mode $_0S_{144}$ (T = 69s) and (right) for the mode $_3S_{105}$ (T = 56s).

Rayleigh and Love overtones to the crust is also important. The large-scale features of crustal corrections predicted by the three different crustal models are generally similar. However, there are differences in the short-scale structures. For example, CRUST2.0 tends to predict more pronounced phase velocity anomalies in regions of thick crust such as in the Tibetan plateau and in the Andes.

3.5. Model Resolution

[16] We carry out Backus-Gilbert resolution tests to assess how well we can resolve isotropic and radially anisotropic structure at different locations in the Earth. We calculate Backus-Gilbert averaging kernels [e.g., *Backus and Gilbert*, 1968; *Menke*, 1989], which describe how the value obtained in the model at a given point is a spatial average over the true structure. Ideally these kernels are delta functions in space, but given the finiteness of model parameterization, incomplete data coverage and the damping applied, these kernels have a finite spatial extent. Figure 6 shows horizontal and vertical cross sections through Backus-Gilbert kernels computed for six locations in the mantle to illustrate the variable isotropic (solid lines) and anisotropic (dashed lines) model resolution. The upper 200 km of the mantle have the highest resolution, decreasing with depth. In the southern hemisphere, where the data coverage is poorer, (e.g., Figure 6f) the depth kernels are not only broader but also have lower amplitude than in regions well covered, reflecting poorer depth resolution. The resolution for radially anisotropic structure is poorer than for isotropic structure. Such poorer resolution prompts us to choose different levels of damping for isotropic and anisotropic parameters.

4. Results

4.1. Misfit Curves for the Data

[17] In order to assess the amount of radial anisotropy required by our data set we carry out joint inversions for isotropic and radially anisotropic structure using a variety of levels of damping. Figure 7 shows data misfit curves for three-dimensional Earth models obtained using various levels of damping for the anisotropic parameters, while keeping the damping of the isotropic parameters constant. We

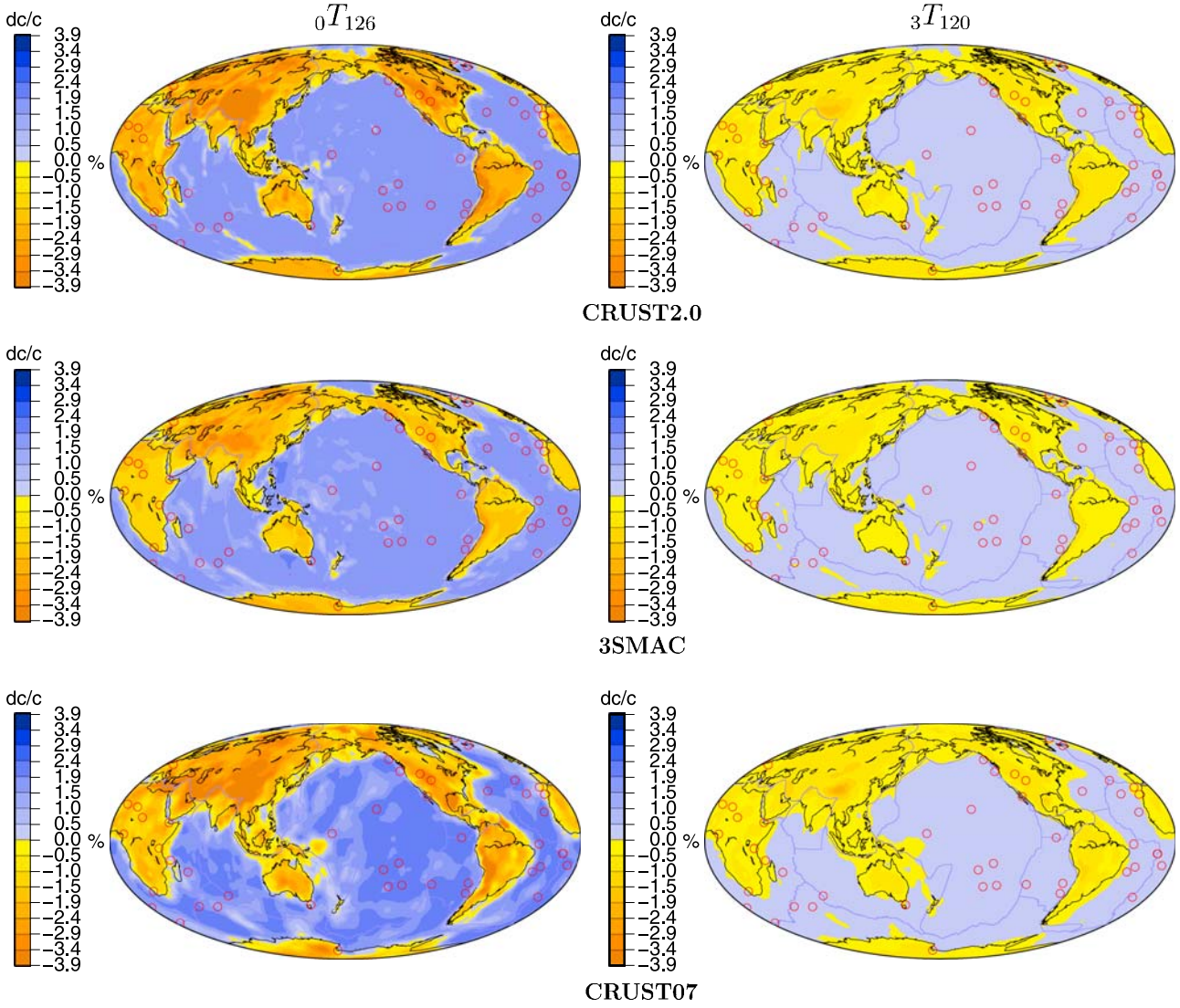

Figure 5. Love wave phase velocity distributions associated with the crustal model (top) CRUST2.0, (middle) 3SMAC and (bottom) CRUST07 (left) for the mode $_0T_{126}$ (T = 69s) and (right) for the mode $_3T_{120}$ (T = 51s). Note that the color scale used here is different than that used in Figure 4.

use the same data set and modeling strategy in all the inversions, only changing the anisotropic damping parameter. All the results are obtained using crustal corrections from CRUST2.0. The data misfit, m^2, is given by:

$$m^2 = \frac{(A\mathbf{x} - \mathbf{d})^T (A\mathbf{x} - \mathbf{d})}{\mathbf{d}^T \mathbf{d}}, \qquad (1)$$

where $\mathbf{x}$ is the solution model, A is the matrix with the data derivatives and $\mathbf{d}$ is the data vector. The data misfit is plotted as a function of the effective number of parameters, which is given by the trace of the resolution matrix. The curve labeled with "1x" corresponds to an inversion where the same level of damping is applied to both isotropic and anisotropic parameters, "2x" means that the anisotropic parameters are damped two times more than the isotropic parameters, and so successively. The solid line (labeled "iso") corresponds to an inversion not allowing deviations of radial anisotropy from PREM. We shall refer to such an inversion as isotropic inversion throughout this paper. Each point on each line corresponds to an Earth model, so Figure 7 we represent over 200 three-dimensional Earth models. As we increase the strength of damping of the anisotropic parameters the misfit increases, with the isotropic models along the solid line having the poorest fit to the data. However, although overall the laterally varying anisotropic models explain the data better than the isotropic ones, the actual differences in misfit are very small; allowing deviations in radial anisotropy from PREM improves the fit to the data by no more than 1.5%.

[18] In the remaining sections we shall compare a variety of three-dimensional isotropic and radially anisotropic mantle models. In order to carry out fair comparisons it is important to make sure that the models have the same effective number of parameters. It is not the purpose of this study to present detailed Earth models, but to assess the robustness of radially anisotropic inversions, so we will focus on long-wavelength models with 1,500 effective parameters. Furthermore, throughout this paper we shall show radially anisotropic

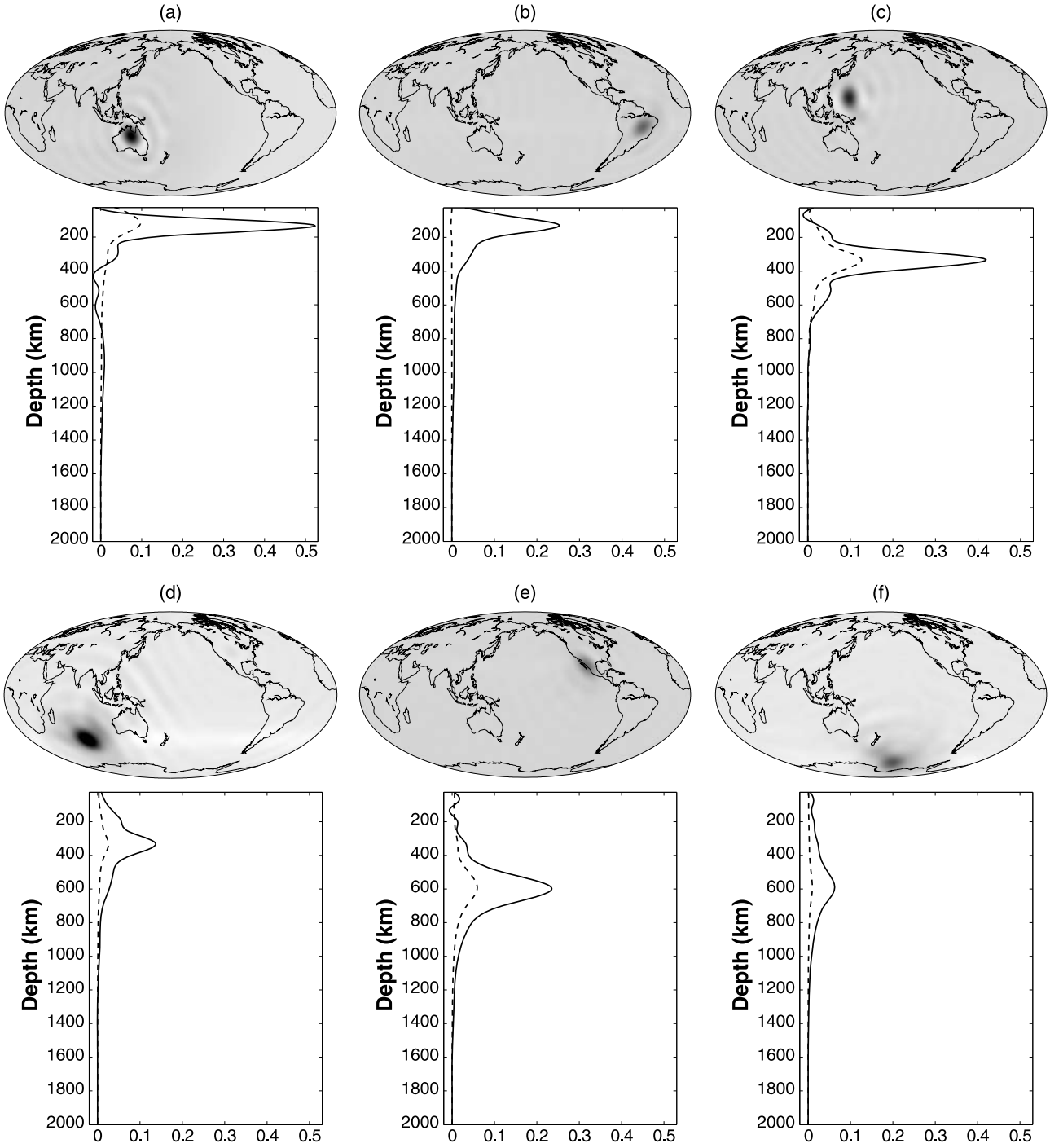

Figure 6. Backus-Gilbert resolution kernels for points beneath (a) Australia (150 km), (b) Brazil (150 km), (c) Mariana Islands (350 km), (d) Indian Ocean (350 km), (e) Western United States (575 km) and (f) Southern Pacific (575 km). Map views of the kernels are shown on the top. The radial dependence of the kernels is shown below each map (solid lines are shear velocity kernels and dashed lines are kernels for radial anisotropy).

models obtained damping the anisotropic parameters two times more than the isotropic parameters.

[19] Figure 8 compares the shear-velocity structure obtained from an isotropic inversion with the isotropic shear-velocity structure obtained from a joint inversion for both isotropic and radially anisotropic Earth structure.

[20] The three-dimensional isotropic shear-velocity structures shown in Figure 8 share the large-scale features of previous global tomographic studies. For example, near the surface the signature of slow ridges and back arc regions is very clear. The continents have deep (≈250 km) keels, which are particularly pronounced in the ancient cratonic regions,

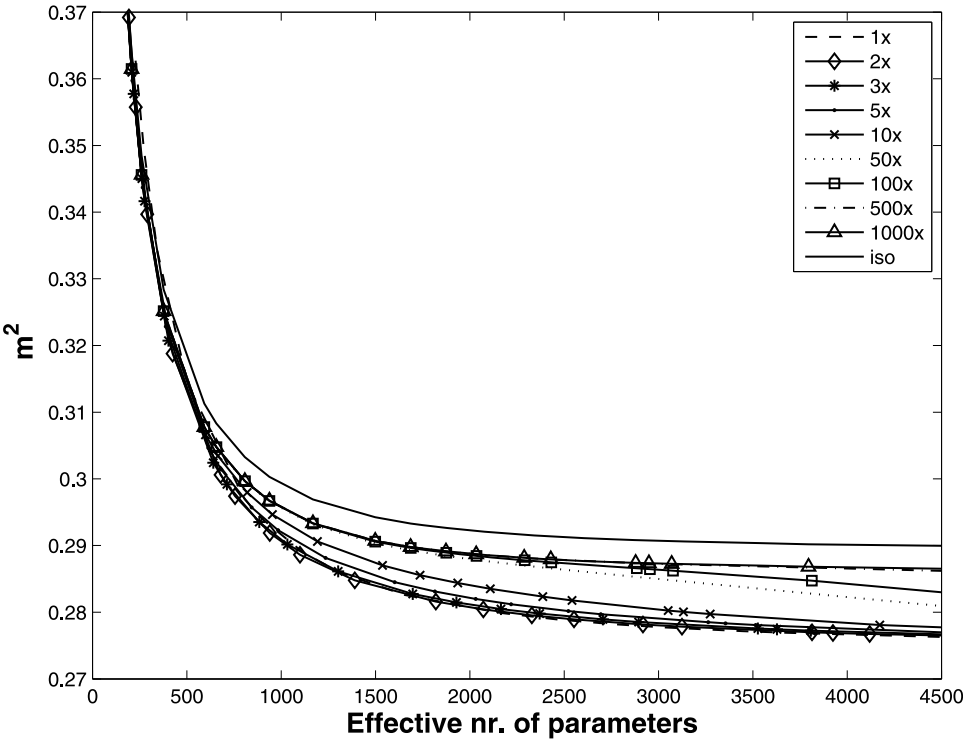

Figure 7. Misfit curves for a variety of 3-D radially anisotropic models obtained using various levels of horizontal gradient damping. "1x" means the same damping has been applied to the isotropic parameters and to the anisotropic parameters. "2x" means the anisotropic parameters have been damped twice more than the isotropic parameters, and so successively. "Iso" corresponds to an inversion where no anisotropy is allowed beyond PREM.

and have the largest anomalies around 100–150 km depth. At depths in excess of 250 km, the magnitude of lateral variations is smaller, and the signature of subduction emerges as one of the clearest signals from a depth of about 400 km, persisting to greater depths. The shear-velocity structure from the isotropic inversion is very compatible with that from a joint inversion for isotropic and anisotropic structure, with some slight differences at depth of 150 km and also at 800 km, where the model resolution is poor.

4.2. Effect of Crustal Corrections

[21] We test the robustness of the anisotropic results by following exactly the same inversion modeling procedure as in section 4.1 for joint determination of isotropic and radially anisotropic structure, but now using not only crustal corrections from CRUST2.0 but also from 3SMAC and from CRUST07.

[22] Figure 9 compares the isotropic shear wave velocity structure of three Earth models with 1,500 effective parameters obtained using the different crustal corrections. The models are similar, with some slight differences in the shallow structure (≈50 km), notably in the Tibetan plateau. At greater depths (≈800 km) there are also differences in structure, but as seen in Figure 6, resolution decreases at great depths. The corresponding radially anisotropic structure obtained using the three different crustal corrections is shown in Figure 10. The large-scale features of radial anisotropy in the three different models agree with each other. At a depth of 150 km a relatively pronounced positive anisotropy anomaly underneath the Pacific emerges, which has been reported in previous studies [*Ekström and Dziewonski*, 1998; *Gung et al.*, 2003; *Panning and Romanowicz*, 2004]. From a depth of around 200 km the models show a negative anisotropy anomaly around the Pacific, particularly under the southeast Pacific. At depths greater than 400 km that pattern diminishes in amplitude and below 600 km the pattern changes again, but at this depth and below the resolution of the data is poor. Although the large-scale features of the anisotropic models are generally compatible with each other there are important differences between them. Figure 11 compares the radially anisotropic models in Figure 10 at a depth of 100 km. It is clear that the three images are quite different, particularly beneath the Pacific and Eurasia.

[23] Changing the crustal corrections from those predicted by CRUST2.0 to those obtained using 3SMAC and CRUST07,

Figure 8. Isotropic shear velocity perturbations from PREM derived (left) from an inversion not allowing deviations of radial anisotropy from PREM and (right) from a joint inversion for isotropic and radially anisotropic structure, using crustal corrections from CRUST2.0. We compare models with 1,500 effective parameters and the data misfits are Figure 8 (left) $m^2 = 0.2942$ for the "isotropic" inversion and Figure 8 (right) $m^2 = 0.2872$ for the anisotropic inversion. The color scale has different ranges at different depths, which are shown at the top of each depth slice.

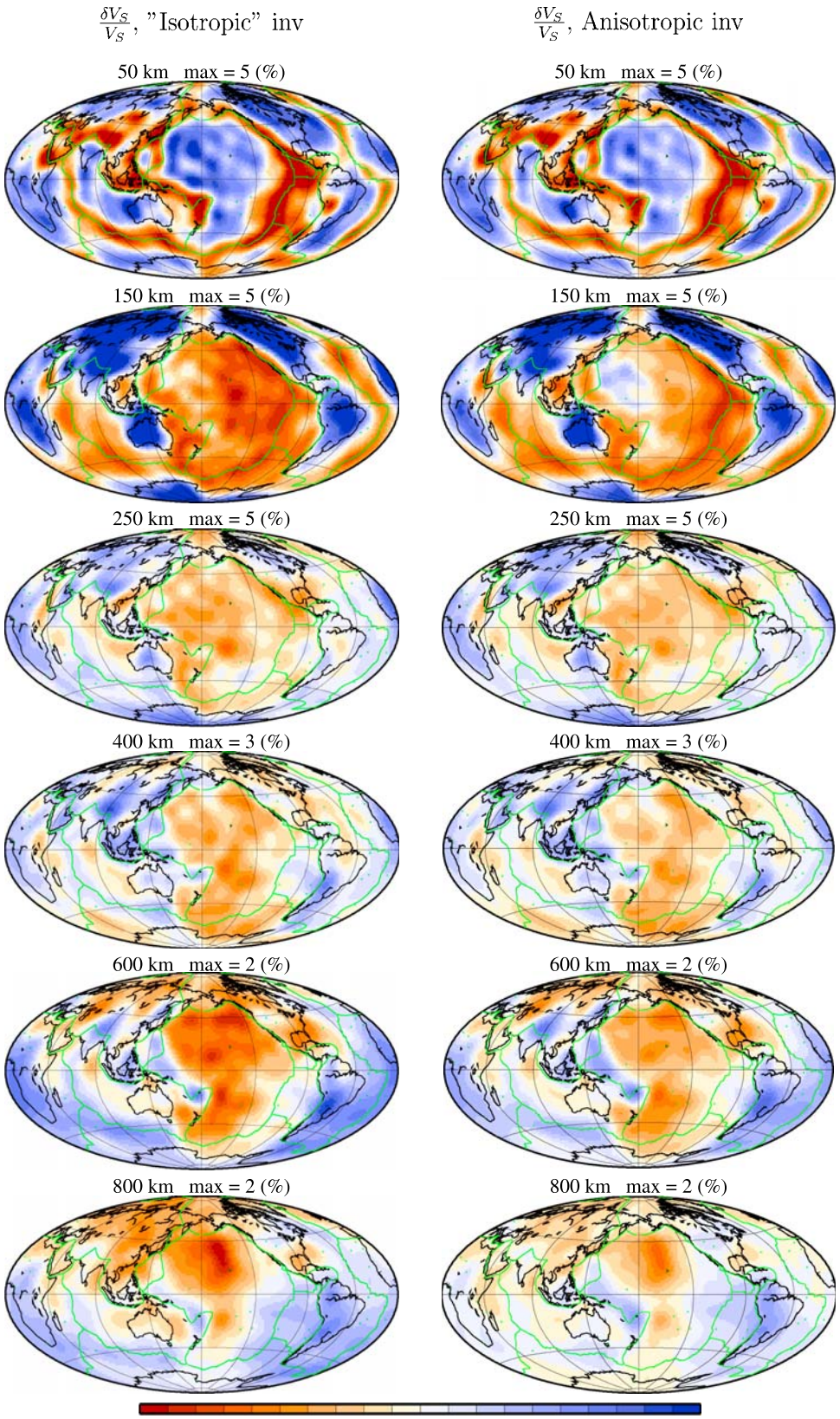
$\frac{\delta V_S}{V_S}$, "Isotropic" inv
$\frac{\delta V_S}{V_S}$, Anisotropic inv
50 km max = 5 (%)
150 km max = 5 (%)
250 km max = 5 (%)
400 km max = 3 (%)
600 km max = 2 (%)
800 km max = 2 (%)

Figure 8

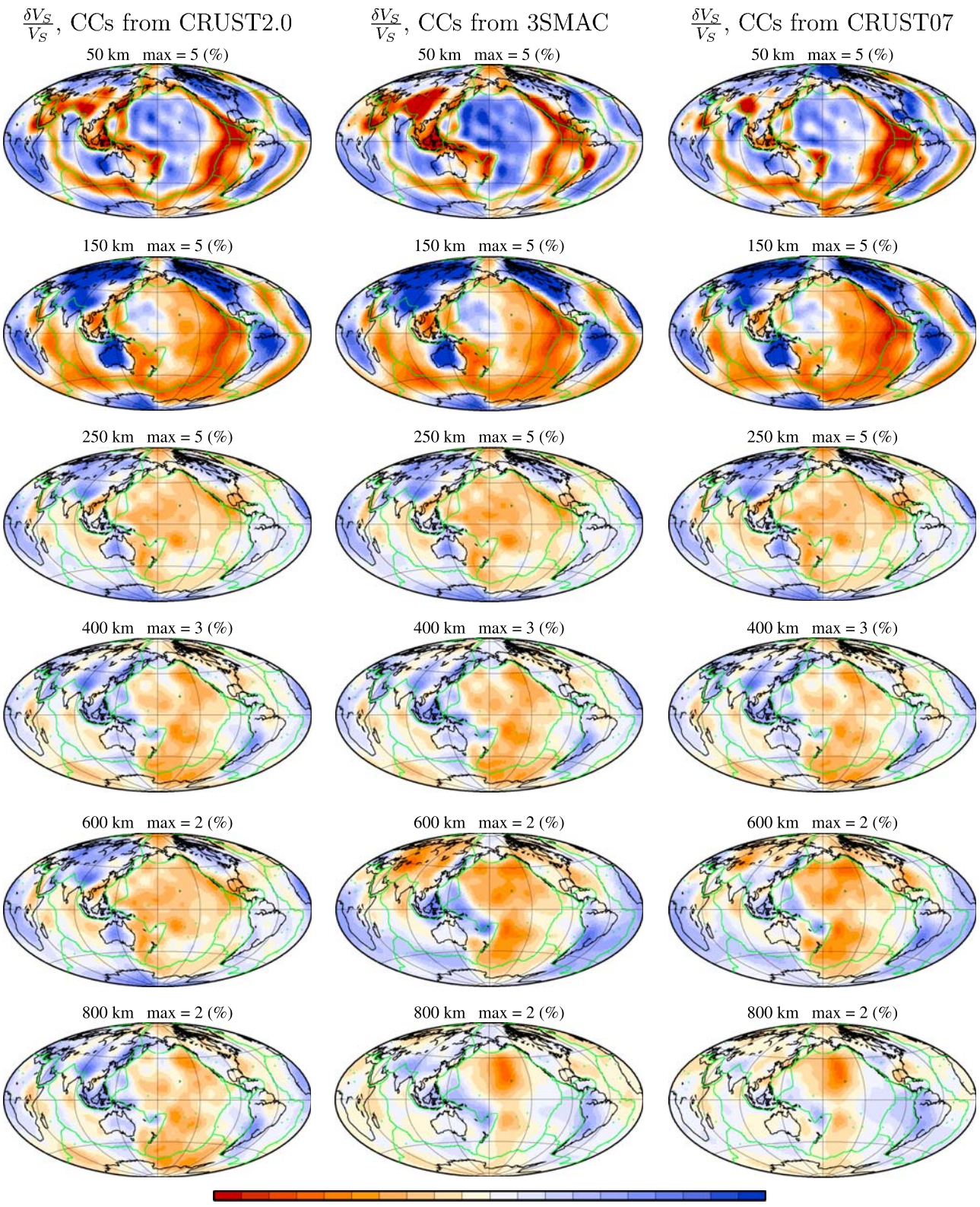

Figure 9. Isotropic shear velocity perturbations from PREM derived from joint inversions for isotropic and radially anisotropic structure using crustal corrections from different models: (left) CRUST2.0, (middle) 3SMAC and (right) CRUST07. We compare models with 1,500 effective parameters and the data misfits are $m^2 = 0.2872$ for the inversion using CRUST2.0, $m^2 = 0.2927$ for the inversion using 3SMAC and $m^2 = 0.3117$ for the inversion using CRUST07. The color scale has different ranges at different depths, which are shown at the top of each depth slice.

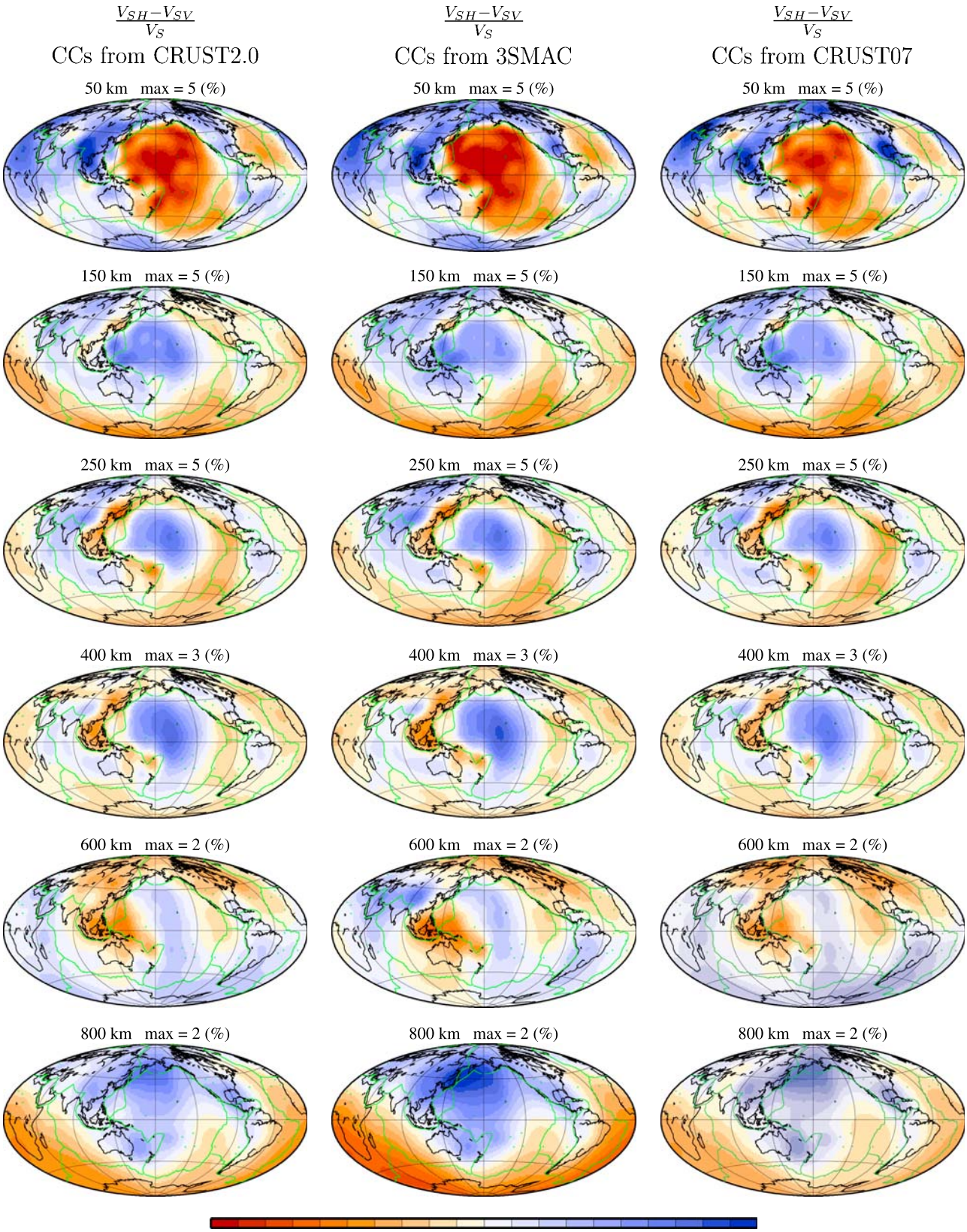

Figure 10. Same as in Figure 9 but for anisotropic velocity variations ($\frac{V_{SH}-V_{SV}}{V_S}$). Average anisotropy at each depth has been removed.

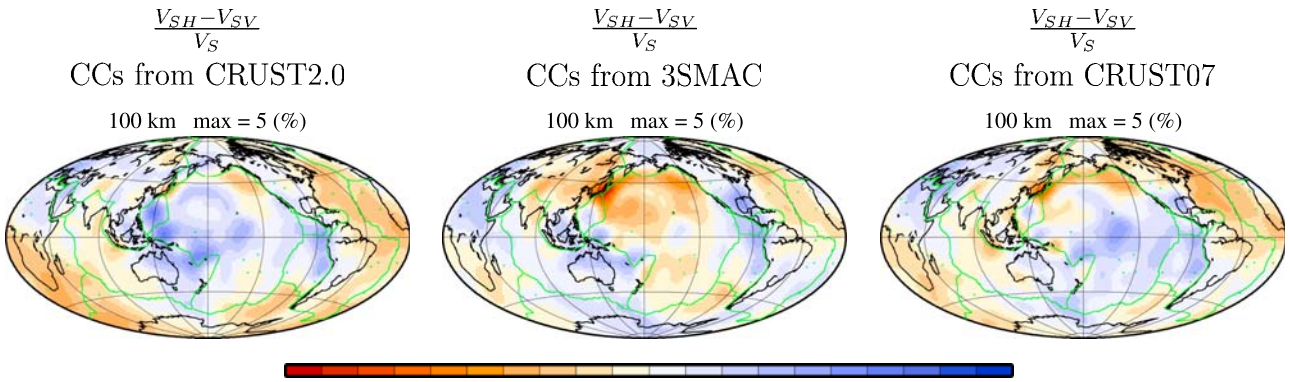

Figure 11. Same as in Figure 10, but for a depth of 100 km.

the data fit deteriorates by about 0.6% and 2%, respectively (for exact numbers see the captions of Figure 9). For example, the radially anisotropic model obtained using crustal corrections from 3SMAC explains the data as well as the isotropic model obtained using crustal corrections from CRUST2.0 (see Figure 8). Thus, using crustal corrections predicted by different crustal models has a similar or larger effect on the data misfit as including laterally varying radial anisotropy in the modeling.

4.3. χ^2 Analysis of Data Misfit

[24] To further assess the differences in data misfit of the various models we carried out inversions minimizing χ^2, defined by:

$$\frac{\chi^2}{N} = \frac{1}{M-K}(d-Ax)^T C_d^{-1}(d-Ax), \qquad (2)$$

where $N = M - K$, M is the total number of data points, K is the effective number of parameters and C_d is the data covariance matrix, which we take to be diagonal. *Visser et al.* [2007a] provide variance estimates derived from their measurement algorithm; we calculate variance estimates for the measurements of *van Heijst and Woodhouse* [1999] and of *Ekström et al.* [1997] using the cluster analysis approach of *Trampert and Woodhouse* [2001]. Errors estimated using cluster analyses assume a Gaussian distribution, which may be inappropriate, so errors in the data are only approximately known. The models obtained by minimizing χ^2 are very similar to those obtained by minimizing the data misfit m^2 (equation (1)). The $\frac{\chi^2}{N}$ values obtained for the 3-D anisotropic models with 1,500 parameters, for a variety of crustal models are: $\frac{\chi^2}{N} = 1.4824$ for CRUST2.0, $\frac{\chi^2}{N} = 1.5153$ for 3SMAC and $\frac{\chi^2}{N} = 1.5343$ for CRUST07. The $\frac{\chi^2}{N}$ value for the 3-D isotropic model with 1,500 parameters is $\frac{\chi^2}{N} = 1.5155$ (using the CRUST2.0 crustal model). These values of $\frac{\chi^2}{N}$ indicate that none of the models explain the data very well, as they are larger than 1. The radially anisotropic models obtained using crustal corrections from 3SMAC and from CRUST07 have a comparable or poorer data fit than the isotropic model obtained using CRUST2.0, confirming the findings from section 4.2 that using different crustal corrections has a similar influence on the data fit to including radial anisotropy in the modeling.

4.4. Influence of P Wave Velocity Variations

[25] As shown in Figure 1 and discussed in section 3.1, Rayleigh waves are also sensitive to variations in P wave velocity and, at least for some modes, this effect can be important. It is common practice to use scaling factors between shear wave velocity and compressional wave velocity to reduce the number of parameters in the inversion process, as we have explained in section 3. In this section we do not use such scaling relation and instead we carry out joint inversions for shear velocity and for compressional velocity perturbations. We use crustal corrections from CRUST2.0, we do not include anisotropy in the inversions and we apply damping to the P velocity structure two times stronger than to the S velocity structure. Figure 12 shows S velocity and P velocity models we obtained with a total of 1,500 effective parameters. The S velocity structure retrieved is consistent with the isotropic shear velocity models shown previously in Figures 8–9. The P velocity model is poorly resolved and has structure at shallow depths (50 km) only, reflecting the sensitivity of Rayleigh waves to P velocity in the top of the upper mantle. The low P velocities obtained under the Western Pacific and Eastern Eurasia are broadly compatible with the shallow mantle structure in existing higher-resolution P wave velocity models [e.g., *Antolik et al.*, 2003].

[26] The data misfit for the model in Figure 12 is $\chi^2/N = 1.5079$, which is slightly lower than the data fit of the isotropic model obtained using crustal corrections from CRUST2.0 ($\frac{\chi^2}{N} = 1.5155$, Figure 9).

5. Discussion and Conclusions

[27] We have shown that imperfect crustal corrections have a similar effect on the data fit to lateral variations in radial anisotropy. In addition, the use of crustal corrections from different *a priori* crustal models may lead to different images of radial anisotropy.

[28] Using crustal corrections from 3SMAC leads to strong negative radial anisotropy variations under Eurasia and the Pacific at a depth of 100 km (Figure 11). The models obtained using crustal corrections from CRUST2.0 and from CRUST07 show less pronounced variations in the same regions. It is

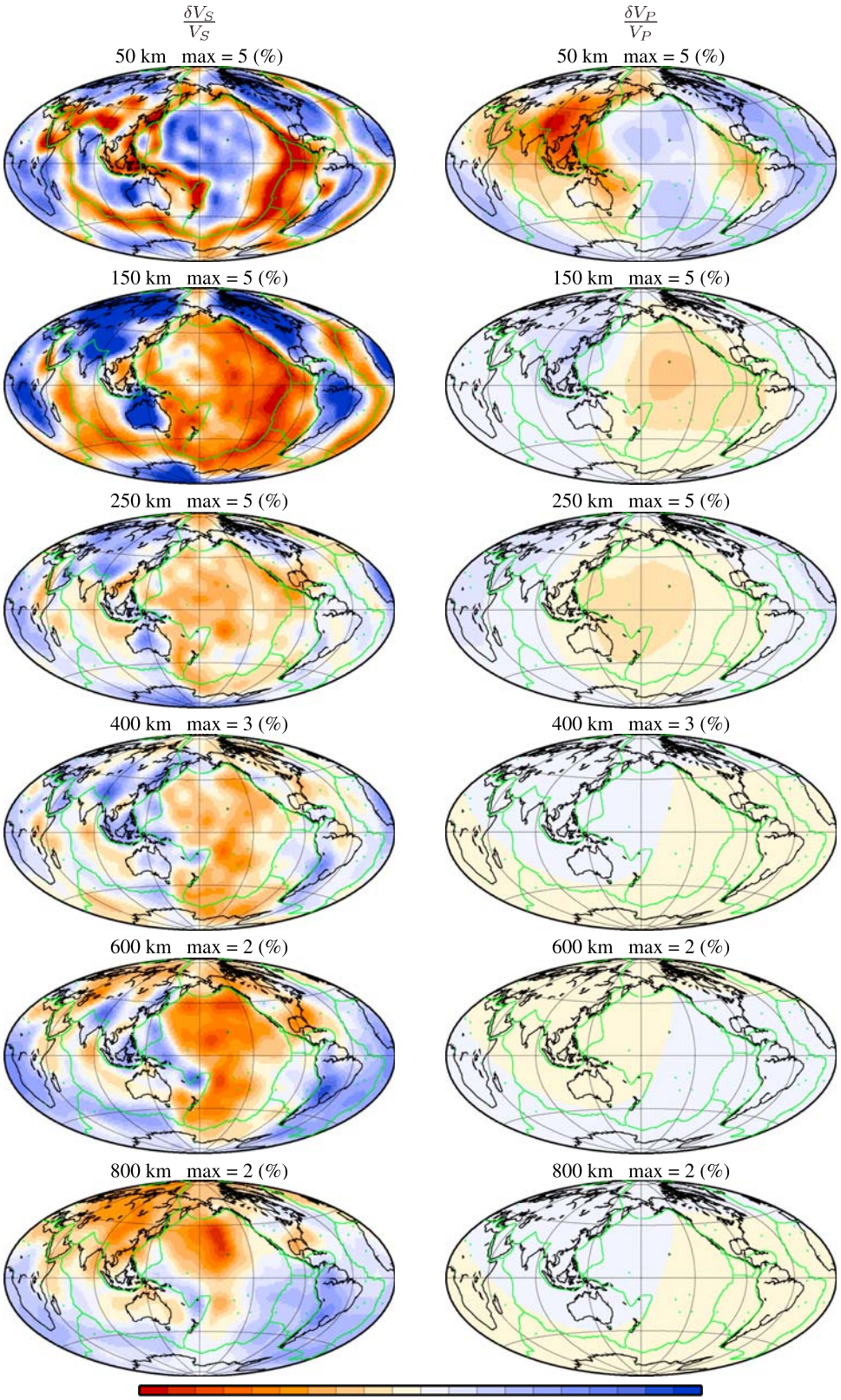

Figure 12. (left) Shear velocity and (right) compressional wave velocity perturbations from PREM jointly determined using crustal corrections from CRUST2.0. This model has 1,500 effective parameters and the data fit is $\chi^2/N = 1.5079$. The color scale has different ranges at different depths, which are shown at the top of each depth slice.

often assumed that the anisotropy at this depth reflects the lithospheric strain field that was "frozen in" at the time of formation of the continental lithosphere, so the different radially anisotropic images at 100 km obtained could lead to divergent interpretations of the processes involved in the generation of continental lithosphere. CRUST07 is a mean crustal model from probability density function distributions [*Meier et al.*, 2007], which is not the best fitting model. This is a possible explanation for the poorest data fit obtained using crustal corrections from CRUST07. In the future it will be interesting to carry out experiments using a variety of crustal models obtained randomly from the distributions and calculate crustal corrections for each of the models. Average crustal corrections could then be obtained with associated standard deviations.

[29] Thorough data misfit analyses of tomographic models with the same effective number of parameters and the assessment of unmodeled effects are necessary to evaluate the robustness of seismic tomographic images. For example, *Kustowski et al.* [2008] compare the data fit for models from inversions including and not including lateral variations in radial anisotropy. Their results show that the inclusion of lateral variations in anisotropy improves the data fit to surface wave dispersion data by relatively small amounts (about 1% except for T = 35s Rayleigh waves, where the fit improves by about 3.5%).

[30] It is clear that lateral variations in radial anisotropy are likely to occur in the interior of the Earth's mantle [e.g., *Visser et al.*, 2008] and that the effort to image the fine details of global anisotropy in the Earth's interior must continue. Careful studies fully investigating the need of anisotropy by the data and assessing the biases by unmodeled effects are essential to obtain images that are reliable for making geodynamic inferences. Such research will very likely benefit from more sophisticated anisotropy modeling techniques [e.g., *Sieminski et al.*, 2007] combined with increased capabilities in both computation and data collection. Moreover, there is scope for progress by combining intermediate and long-period surface waves with other types of data able to resolve the shallow crust, including short-period surface wave group velocity measurements, receiver functions, as well as recent ambient noise and array-based earthquake measurements.

[31] **Acknowledgments.** AMGF thanks funding from NERC postdoctoral fellowship under grant NE/C510916/1 and from Royal Society grant 2007/R2. This research was also funded by the European Commission's Human Resources and Mobility Programme Marie Curie Research Training Network SPICE contract MRTN-CT-2003-504267. We gratefully acknowledge the availability of global seismograms from the IRIS/IDA/USGS and GEOFON networks and the IRIS Data Centre. Data and computing facilities at Oxford have been supported under NERC grants NER/F/S/2001/00369 and NE/B505997/1. Part of the research presented in this paper was carried out on the High Performance Computing Cluster supported by the Research Computing Service at the University of East Anglia.

References

Aki, K., and K. Kaminuma (1963), Phase velocity of love waves in Japan, Part i: Love waves from the Aleutian shock of March 1957, *Bull. Earthquakes Res. Inst. Univ. Tokyo*, *41*, 243–259.

Anderson, D. L. (1961), Elastic wave propagation in layered anisotropic media, *J. Geophys. Res.*, *66*, 2953–2963.

Anderson, D. L., E. Schreiber, R. C. Liebermann, and N. Soga (1968), Some elastic constant data on minerals relevant to geophysics, *Rev. Geophys.*, *6*, 491–524.

Antolik, M., Y. Gu, G. Ektsröm, and A. Dziewonski (2003), J362D28: A new joint model of compressional and shear velocity in the Earth's mantle, *Geophys. J. Int.*, *153*, 443–466.

Backus, G. E., and J. F. Gilbert (1968), The resolving power of gross Earth data, *Geophys. J. R. Astron. Soc.*, *16*, 169–205.

Bassin, C., G. Laske, and G. Masters (2000), The current limits of resolution for surface wave tomography in North America, *EOS Trans. AGU*, *F897*, 81.

Bozdag, E., and J. Trampert (2007), On crustal corrections in surface wave tomography, *Geophys. J. Int.*, *172*(3), 1076–1088.

Dziewonski, A. M., and D. Anderson (1981), Preliminary Reference Earth Model, *Phys. Earth Planet. Inter.*, *25*, 297–356.

Ekström, G., and A. M. Dziewonski (1998), The unique anisotropy of the Pacific upper mantle, *Nature*, *394*, 168–172.

Ekström, G., J. Tromp, and E. W. F. Larson (1997), Measurements and global models of surface wave propagation, *J. Geophys. Res.*, *102*, 8137–8157.

Gung, Y., M. Panning, and B. Romanowicz (2003), Global anisotropy and the thickness of continents, *Nature*, *422*, 707–711.

Kustowski, B., G. Ekström, and A. M. Dziewonski (2008), Anisotropic shear-wave velocity structure of the earth's mantle: A global model, *J. Geophys. Res.*, *113*, B06306, doi:10.1029/2007JB005169.

Love, A. E. H. (1927), *A Treatise on the Theory of Elasticity*, Cambridge Univ. Press, Cambridge, U. K.

Marone, F., and B. Romanowicz (2007), Non-linear crustal corrections in high-resolution waveform seismic tomography, *Geophys. J. Int.*, *170*, 460–467.

Marone, F., Y. C. Gung, and B. Romanowicz (2007), High resolution 3D radial anisotropic structure of the North American upper mantle from inversion of surface waveform data, *Geophys. J. Int.*, *171*, 206–222.

McEvilly, T. V. (1964), Central U.S. crust-upper mantle structure from Love and Rayleigh wave phase velocity inversion, *Bull. Seismol. Soc. Am.*, *54*, 1997–2015.

McNamara, A., P. van Keken, and S. Karato (2002), Development of anisotropic structure by solid-state convection in the Earth's lower mantle, *Nature*, *416*, 310–314.

Meier, U., A. Curtis, and J. Trampert (2007), Fully nonlinear inversion of fundamental mode surface waves for a global crustal model, *Geophys. Res. Lett.*, *34*, L16304, doi:10.1029/2007GL030989.

Menke, W. (1989), *Geophysical Data Analysis: Discrete Inverse Theory*, 2nd ed., Academic, New York.

Montagner, J. P., and T. Tanimoto (1991), Global upper mantle tomography of seismic velocities and anisotropies, *J. Geophys. Res.*, *96*, 20,337–20,351.

Nataf, H. C., and Y. Ricard (1996), 3SMAC: An a priori tomographic model of the upper mantle based on geophysical modeling, *Phys. Earth Planet. Inter.*, *95*, 101–122.

Nataf, H. C., I. Nakanishi, and D. L. Anderson (1984), Anisotropy and shear-velocity heterogeneities in the upper mantle, *Geophys. Res. Lett.*, *11*, 109–112.

Nataf, H. C., I. Nakanishi, and D. L. Anderson (1986), Measurements of mantle wave velocities and inversion for lateral heterogeneities and anisotropy.3.Inversion, *J. Geophys. Res.*, *91*, 7261–7307.

Panning, M., and B. Romanowicz (2004), Inference on flow at the base of Earth's mantle based on seismic anisotropy, *Science*, *303*, 351–353.

Pasyanos, M. E., and W. R. Walter (2002), Crust and upper-mantle structure of North Africa, Europe and the Middle East from inversion of surface waves, *Geophys. J. Int.*, *149*(2), 463–481.

Ritsema, J., H. van Heijst, and J. Woodhouse (1999), Complex shear wave velocity structure imaged beneath Africa and Iceland, *Science*, *286*, 1925–1928.

Robertson, G., and J. Woodhouse (1995), Evidence for proportionality of P and S heterogeneity in the lower mantle, *Geophys. J. Int.*, *123*, 85–116.

Shapiro, N. M., and M. Ritzwoller (2002), Monte-carlo inversion for a global shear velocity model of the crust and upper mantle, *Geophys. J. Int.*, *151*, 88–105.

Shapiro, N., M. Ritzwoller, P. Molnar, and V. Levin (2004), Thinning and flow of tibetan crust constrained by seismic anisotropy, *Science*, *305*, 233–236.

Sieminski, A., Q. Liu, J. Trampert, and J. Tromp (2007), Finite-frequency sensitivity of surface waves to anisotropy based upon adjoint methods, *Geophys. J. Int.*, *168*, 1153–1174.

Silver, P. G. (1996), Seismic anisotropy beneath the continents: Probing the depths of geology, *Ann. Rev. Earth Planet. Sci.*, *24*, 385–432.

Takeuchi, H., and M. Saito (1972), Seismic surface waves, *Methods Comput. Phys.*, *11*, 217–295.

Trampert, J., and J. H. Woodhouse (2001), Assessment of global phase velocity maps, *Geophys. J. Int.*, *144*, 165–174.

van Heijst, H. J., and J. H. Woodhouse (1999), Global high-resolution phase velocity distributions of overtone and fundamental-mode surface waves determined by mode branch stripping, *Geophys. J. Int.*, *137*, 601–620.

Vinnik, L. P., L. I. Makeyeva, A. Milev, and Y. Usenko (1992), Global patterns of azimuthal anisotropy and deformation in the continental mantle, *Geophys. J. Int.*, *111*, 433–447.

Visser, K., S. Lebedev, J. Trampert, and B. L. N. Kennett (2007a), Global love wave overtone measurements, *Geophys. Res. Lett.*, *34*, L03302, doi:10.1029/2006GL028671.

Visser, K., J. Trampert, and B. L. N. Kennett (2007b), Global anisotropic phase velocity maps for higher mode Love and Rayleigh waves, *Geophys. J. Int.*, *172*, 1016–1032.

Visser, K., J. Trampert, S. Lebedev, and B. L. N. Kennett (2008), Probability of radial anisotropy in the deep mantle, *Earth Planet. Sci. Lett.*, *270*, 241–250.

Williams, Q., and E. Garnero (1996), Seismic evidence for partial melt at the base of earth's mantle, *Science*, *273*, 1528–1530.

Woodhouse, J. H., and A. M. Dziewonski (1984), Mapping the upper mantle: Three dimensional modeling of earth structure by inversion of waveforms, *J. Geophys. Res.*, *89*, 5953–5986.

Yang, Y., M. Ritzwoller, F.-C. Lin, M. Moschetti, and N. Shapiro (2008), The structure of the crust and uppermost mantle beneath the western us revealed by ambient noise and earthquake tomography, *J. Geophys. Res.*, *113*, B12310, doi:10.1029/2008JB005833.

A. M. G. Ferreira, School of Environmental Sciences, University of East Anglia, Norwich NR4 7TJ, UK. (a.ferreira@uea.ac.uk)

J. Trampert, Department of Earth Sciences, Utrecht University, PO Box 80021, NL-3508 TA, Utrecht, Netherlands. (jeannot@geo.uu.nl)

K. Visser, Built Environment and Geosciences, TNO, NL-3584 CB, Utrecht, Netherlands. (karin.vanthienen@tno.nl)

J. H. Woodhouse, Department of Earth Sciences, University of Oxford, Parks Road, Oxford OX1 3PR, UK. (john.woodhouse@earth.ox.ac.uk)